
Article:
Finizio, S, Wintz, S, Zeissler, K et al. (5 more authors) (2018) Dynamic imaging of the delay- and tilt-free motion of Néel domain walls in perpendicularly magnetized superlattices. Nano Letters, 19 (1). pp. 375-380. ISSN 1530-6984

https://doi.org/10.1021/acs.nanolett.8b04091

Dynamic imaging of the delay- and tilt-free motion of Néel domain walls in perpendicularly magnetized superlattices

S. Finizio,[*,†] S. Wintz,[†,§] K. Zeissler,[‡] A. V. Sadovnikov,[¶,‖] S. Mayr,[†,⊥] S. A. Nikitov,[¶,‖] C. H. Marrows,[‡] and J. Raabe[†]

Swiss Light Source, Paul Scherrer Institut, 5232 Villigen PSI, Switzerland, School of Physics and Astronomy, University of Leeds, Leeds LS2 9JT, United Kingdom, and Laboratory Metamaterials, Saratov State University, Saratov, 410012, Russia

E-mail: simone.finizio@psi.ch

KEYWORDS: current-induced domain wall motion, field-induced domain wall motion, magnetization dynamics, time-resolved x-ray microscopy

Abstract

We report on the time-resolved investigation of current- and field-induced domain wall motion in the flow regime in perpendicularly magnetized microwires exhibiting anti-symmetric exchange interaction by means of scanning transmission x-ray microscopy using a time step

[*]To whom correspondence should be addressed

[†]Swiss Light Source, Paul Scherrer Institut, 5232 Villigen PSI, Switzerland

[‡]School of Physics and Astronomy, University of Leeds, Leeds LS2 9JT, United Kingdom

[¶]Laboratory Metamaterials, Saratov State University, Saratov, 410012, Russia

[§]Institute of Ion Beam Physics and Materials Research, Helmholtz-Zentrum Dresden-Rossendorf, 01328 Dresden, Germany

[‖]Kotel'nikov Institute of Radioengineering and Electronics, Russian Academy of Sciences, Moscow, 125009, Russia

[⊥]Department of Materials, Laboratory for Mesoscopic Systems, ETH Zürich, 8093 Zürich, Switzerland

of 200 ps. The sub-ns time step of the dynamical images allowed us to observe the absence of incubation times for the motion of the domain wall within an uncertainty of 200 ps, together with indications for a negligible inertia of the domain wall. Furthermore, we observed that, for short current and magnetic field pulses, the magnetic domain walls do not exhibit a tilting during its motion, providing a mechanism for the fast, tilt-free, current-induced motion of magnetic domain walls.

Since the first observations that electrical currents can induce the motion of magnetic domain walls (current induced domain wall motion - CIDWM) through the spin transfer torque effect[1,2], many different mechanisms that allow for the motion of magnetic domain walls by electrical currents have been discovered. In particular, the discovery that spin-orbit torques can displace magnetic domain walls[3–9] has allowed for the achievement of fast domain wall motion velocities (up to several hundreds of meters per second) in multilayer superlattice stacks optimized for both a high perpendicular magnetic anisotropy (PMA) and a large anti-symmetric exchange interaction (or Dzyaloshinskii-Moriya - DM - interaction). These discoveries have allowed for the development and optimization of magnetic memory concepts based on CIDWM such as e.g. the racetrack memory[6].

The unraveling of the domain wall motion dynamics at the ns and sub-ns timescale is of paramount importance for the understanding of the physical processes governing their motion, such as e.g. the acceleration/deceleration of the domain wall at the start/end of the application of the electrical current (i.e. the inertia of the domain wall)[8,10], the effect of the DM interaction on the shape of the domain wall during its motion[11,12], and the differences between current- and field-induced domain wall motion (FIDWM)[11,12]. Furthermore, the understanding of the dynamical processes is required in order to validate the theoretical models (such as e.g. the 1D model[5]) currently employed for the description of the CIDWM and FIDWM processes.

The experimental investigation of the sub-ns dynamics of the CIDWM and FIDWM processes requires a non-invasive microscopy technique combining a high spatial and temporal resolution (in the pump-probe regime) with an insensitivity to electric and magnetic fields, and with the possi-

bility to acquire time-resolved images with sub-ns time steps. Only a few time-resolved studies of the CIDWM process exist[8], but they are limited in time step of the time-resolved images (in Ref.[8], time steps on the order of 5-20 ns are employed) and in the magnitude of the applicable current densities (due to the use of photoemission electron microscopy - PEEM, which is extremely sensitive to variations in the surface potential of the sample[13], as the probing technique). This leaves open questions on the presence of dynamical processes on the ns and sub-ns timescale at the beginning of the motion of the domain wall (i.e. on timescales where most magneto-dynamical processes are expected to occur), and on the presence of a fast acceleration which cannot be observed with the time-step employed for the experiments reported in Ref.[8].

In this letter, we report on the time-resolved investigation of the CIDWM and FIDWM processes in a Pt/$Co_{68}B_{32}$/Ir microwire using time-resolved scanning transmission x-ray microscopy (STXM). Time-resolved images of the dynamics of the CIDWM and FIDWM processes employing a time step of 200 ps were successfully acquired, and we could observe an indication of negligible inertia of the domain wall, along with the absence of a tilt of the domain wall when applying short current/field pulses.

Microstructured thin film wires of 2 μm width were fabricated by electron beam lithography followed by liftoff out of a Ta(3.2 nm)/Pt(2.6 nm)/[$Co_{68}B_{32}$(0.8 nm)/Ir(0.4 nm)/Pt(0.6nm)]$_{\times 3}$/Pt(2.1 nm) multilayer superlattice stack deposited by sputtering (details on the deposition of a similar multilayer superlattice stack are given in Ref.[14]). The microwires were fabricated on top of a 200 nm thick x-ray transparent Si_3N_4 membrane on a 200 μm thick high resistivity Si frame. The microwires were contacted by 200 nm thick Cu electrodes fabricated by electron-beam lithography followed by a lift-off process. To generate the magnetic field pulses employed for the reset of the original magnetic state, an Ω-shaped, 400 nm thick, Cu coil was fabricated on top of the microwire by electron-beam lithography followed by a lift-off process. The electrical insulation between the microwire and the Ω-shaped coil is guaranteed by a 200 nm thick SiO_2 layer, deposited by electron-beam evaporation, between the microwire and the coil. A scanning electron micrograph of the sample is shown in Figure 1.

The measurements of the CIDWM and FIDWM dynamics were carried out in a region of the Pt/$Co_{68}B_{32}$/Ir microwire where the current density is uniformly distributed across the microwire, as verified by finite element simulations of the current flow (area marked by ROI in Figure 1). Due to the contribution from the interfacial DM interaction[14], the Pt/$Co_{68}B_{32}$/Ir multilayered superlattices stabilize Néel-type domain walls. Due to the low number of repeats, it is expected that the chirality of the Néel-type domain wall will be the same for all of the three layers[15]. We verified this statement by conducting micromagnetic simulations of a Néel-type domain wall stabilized in the Pt/$Co_{68}B_{32}$/Ir stack employing the finite difference micromagnetic simulation package MuMax3[16]. For the simulations, a saturation magnetization of M_s = 665 kA m^{-1}, a PMA of k = 600 kJ m^{-3}, and a value of D = 1.17 mJ m^{-2} for the DM interaction were selected. These values were determined by magnetometry and Brillouin Light Scattering measurements from a Pt/$Co_{68}B_{32}$/Ir film grown in parallel to the ones that were investigated by time-resolved STXM. A simulation grid of $0.1\times0.1\times0.1$ nm^3 was employed for the simulations. Three magnetic layers of 0.8 nm thickness separated by non-magnetic layers of 1 nm thickness were simulated, using the same set of boundary conditions employed in Ref.[15]. The result of the micromagnetic simulations is shown in Figure 2(d), where it is possible to observe that a Néel-type domain wall of the same chirality is stabilized in all of the three layers of the Pt/$Co_{68}B_{32}$/Ir film.

The dynamics of the CIDWM and FIDWM processes were imaged using STXM at the PolLux (X07DA) endstation of the Swiss Light Source[17]. A Fresnel zone plate with an outermost zone width of 25 nm was employed for the measurements presented here. The widths of the entrance and exit slits to the monochromator were selected to achieve a spatial resolution on the order of 25 nm. Magnetic contrast was achieved by the x-ray magnetic circular dichroism (XMCD) effect[18] by tuning the circularly-polarized x-rays to the Co L_3 absorption edge (about 778 eV). The quasi-static images (e.g. Figure 2) were obtained by acquiring two images with opposite photon helicities, and calculating the XMCD contrast by subtracting the two images. Pump-probe time-resolved images were acquired employing circularly-polarized photons with negative helicity, with a broadband avalanche photodiode detector combined with a dedicated field-programmable

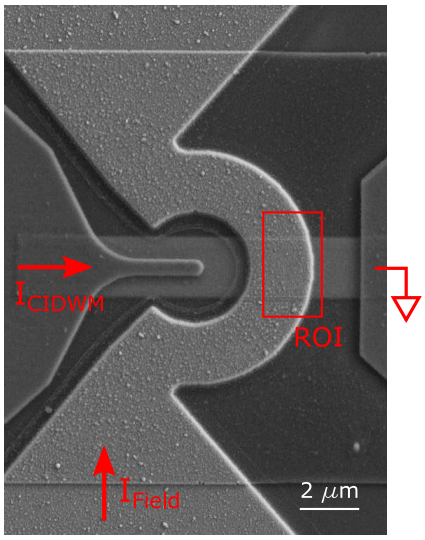

Figure 1: Scanning electron micrograph of the Pt/$Co_{68}B_{32}$/Ir microwire employed for the experiments presented here. A current pulse is injected from the left-hand electrode, with the right-hand electrode at the sample ground, and an out-of-plane magnetic field pulse is generated by injecting a current pulse across the Ω-shaped coil fabricated on top of the microwire. The microwire and the Ω-shaped coil are electrically insulated through a SiO_2 layer. The area investigated in the experiments reported here (region of interest - ROI) is marked by a red rectangle in the figure. The red arrows in the figure indicate the conventional current flow direction.

gate array setup[19,20]. A time step of 200 ps was employed for the time-resolved measurements presented in this letter. The time position of the zero delay between pump and probe (also referred to as t_0) was determined with a fast laser diode connected to the same electronic setup employed for the excitation. The calibration of t_0 allowed for an accuracy of below 200 ps in the synchronization between the excitation signal and the recorded dynamical processes. The jitter between the pump and probe signals was measured to be below 100 ps, therefore guaranteeing that the temporal resolution of the measurements presented here will be limited by the FWHM of the x-ray pulses generated by the synchrotron light source (about 50-70 ps). Thanks to the use of a broadband avalanche photodiode as photon detector, the entire filling pattern of the synchrotron light source could be employed for the acquisition of the time-resolved images, allowing for the possibility to acquire them, under otherwise equal conditions, with a much finer time step than techniques that rely only on the isolated camshaft bunch of the synchrotron light source as probing signal[19,20].

To guarantee the reproducibility necessary for carrying out pump-probe measurements, the fol-

lowing experimental protocol, shown in Figure 2 with static XMCD-STXM images, was adopted: the sample was prepared in its original state by saturating it with a static magnetic field (of about 200 mT, well above the coercive field of the Pt/$Co_{68}B_{32}$/Ir multilayer), and ten thousand 4 ns-long pulses with a peak current of 350 mA were injected across the Ω-shaped coil (see the supplementary information for the simulation of the magnetic field generated by such current pulses), leading to the magnetic state shown in Figure 2(a). Following the initialization of the sample, the time-resolved measurements were carried out with the following procedure: (i) a 5 ns long current pulse, leading to a peak current density of $9 \cdot 10^{11}$ A m^{-2}, was injected across the microwire, leading to a current-induced displacement of the domain wall (Figure 2(b)); (ii) a 4 ns-long, 350 mA, current pulse was injected across the Ω-shaped coil, leading to the generation of a magnetic field that displaced the domain wall back to its original position (Figure 2(c)).

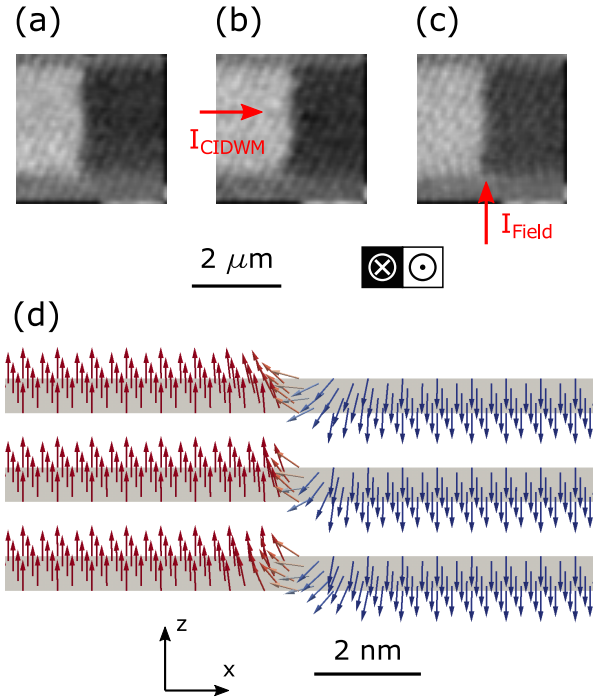

Figure 2: Quasi-static XMCD-STXM images of (a) the initial magnetic configuration, obtained by generating several magnetic field pulses with the Ω-shaped coil; (b) motion of the magnetic domain wall caused by the injection of a 5 ns current pulse across the Pt/$Co_{68}B_{32}$/Ir microwire; (c) Restoration of the initial magnetic configuration by generating one magnetic field pulse with the Ω-shaped coil. (d) Micromagnetic simulation of a domain wall in a three-layer Pt/$Co_{68}B_{32}$/Ir superlattice stack, where it is possible to observe that the domain wall is Néel-type, with the same chirality across all three layers.

From the quasi-static XMCD-STXM investigation of the CIDWM and FIDWM processes shown in Figure 2, it can be observed that the magnetic domain wall is displaced along the direction of the electrical current (i.e. opposite to the direction of the electron flow). This is in agreement with the expectation of the contribution of the spin-orbit torques to the domain wall motion (caused by the spin Hall effect, leading to the generation of a transverse spin current in the heavy metal present in the multilayered superlattice stack)[3–8]. For a 5 ns-long current pulse, a displacement of about 250 nm was observed for the magnetic domain wall, leading to an average CIDWM velocity of 50 m s^{-1}, in agreement with the observed velocities for magnetic domain walls in the flow regime in similar multilayer superlattice stacks[4,7–9]. For the FIDWM process, the domain wall was displaced back to its original position by a 4 ns-long magnetic field pulse, leading to an estimation of about 60 m s^{-1} for the domain wall velocity. This result, as will be described in the next sections of this letter, is however a lower-limit estimation of the true domain wall velocity. It is worth to note here that the presence of a pinning site, which does not however affect the motion of the domain wall in the rest of the microwire, at the lower edge of the microwire can be observed in Figure 2(b).

Figure 3 shows snapshots of a time-resolved image of the CIDWM and FIDWM processes (2 ns time step - see the supplementary information for the time-resolved movies, both with 2 ns and 200 ps time steps). Within the limitations of the pump-probe technique (i.e. non-reproducible stochastic components in the domain wall motion will not be visible in the image), a reproducible back and forth motion of the magnetic domain wall with the magnetic field and current pulses respectively can be observed in the time-resolved images. In order to better visualize the domain wall motion, the images shown in Figure 3 show the difference in the magnetic configuration at each time step with respect to the magnetic configuration of the microwire before the excitation - for (a) given by the current pulse injected across the microwire, and for (b) given by the magnetic field pulse (see supplementary information for additional details on the calculation of the difference images shown in Figure 3). In contrast to XMCD-PEEM imaging, STXM is insensitive to the surface potential of the material, therefore allowing us to investigate the domain wall motion at

high current densities without the image distortions and losses of focus present for PEEM imaging of microwires under an applied voltage difference[8].

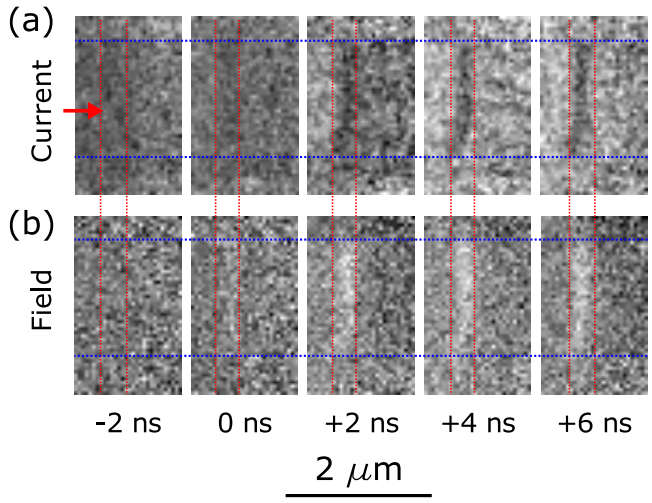

Figure 3: Snapshots at different time delays of (a) the CIDWM (the direction of the applied current is marked by a red arrow in the figure) and (b) the FIDWM processes (the time-resolved movies can be found in the supplementary information). The snapshots are shown as differential images. The edges of the microwire are marked by blue dashed lines in the figure. The red dashed lines indicate the extreme positions of the domain wall.

Additional information on the domain wall motion dynamics can be gathered by determining the change in the XMCD contrast over a CIDWM/FIDWM excitation cycle, calculated by integrating the XMCD contrast in the area where the domain wall displacement is observed (marked by the red dashed lines in Figure 3) for each time step. These results are shown in Figure 4 for both the CIDWM (Figure 4(a)) and FIDWM (Figure 4(b)) processes. An immediately observable difference between the dynamics of the CIDWM and FIDWM processes is that the current-induced motion of the domain wall stops at the end of the current pulse, while the field-induced motion stops before the end of the magnetic field pulse (about 2.4 ns after the start of the 4 ns-long pulse). This difference underlines a different average domain wall velocity for the CIDWM and FIDWM processes, of about 50 m s^{-1} at a peak current density of $9 \cdot 10^{11}$ A m^{-2} for the CIDWM, and of about 100 m s^{-1} for the FIDWM at a peak magnetic field of about 70 mT (see the simulations shown in the supplementary information). The absence of motion after 2.4 ns from the start of the magnetic field pulse can be explained if one considers the distribution of the magnetic field gen-

erated by the Ω-shaped coil, shown in the supplementary information. The spatial distribution of the out-of-plane magnetic field generated by the Ω-shaped coil provides a minimum in the energy for the position of the magnetic domain wall and, once the domain wall reaches that position, the motion will halt (see the supplementary information for a demonstration of this statement based on a simplified one-dimensional model of the Zeeman contribution to the magnetic free energy of the system reported here). This result underlines that, for FIDWM processes, the determination of the domain wall velocity from quasi-static measurements (i.e. distance traveled by the domain wall divided by the pulse width) only provides a lower-limit estimate of the domain wall velocity, and that dynamical measurements are necessary for its correct estimation. It is worth to note here that the oscillations of the recorded contrast after the magnetic field pulse in Figure 4(b) are a measurement artifact due to the cross talk between the Ω-shaped coil and the avalanche photodiode detector of the STXM setup.

For both the CIDWM and FIDWM processes, the motion of the domain wall starts synchronously with the current or field excitation, at least within the available time step of 200 ps. The observation of the absence of an incubation time for the motion of the domain walls provides a strong confirmation that the Néel domain walls stabilized in the Pt/$Co_{68}B_{32}$/Ir PMA multilayer superlattice stack reported here exhibit a negligible inertia, with an improvement of over one order of magnitude in the estimation if compared to previous observations on Pt/Co/AlO_x thin films[8]. This observation is further backed by the sudden halt of the domain wall motion at the end of the current pulse, indicating a fast deceleration of the domain wall (see Figure 4(a)). In addition, no dynamical processes on the ns and sub-ns timescale (besides the motion of the domain wall itself) were observed both at the onset and at the end of the current and magnetic field pulses. As these are the timescales of typical magneto-dynamical processes, our experiments allow us to reliably rule out the presence of additional dynamical processes with a much higher degree of certainty than previous experiments.

Furthermore, as shown in Figure 3 and in the time-resolved movies in the supplementary information, the magnetic domains do not appear to tilt during their displacement induced either by

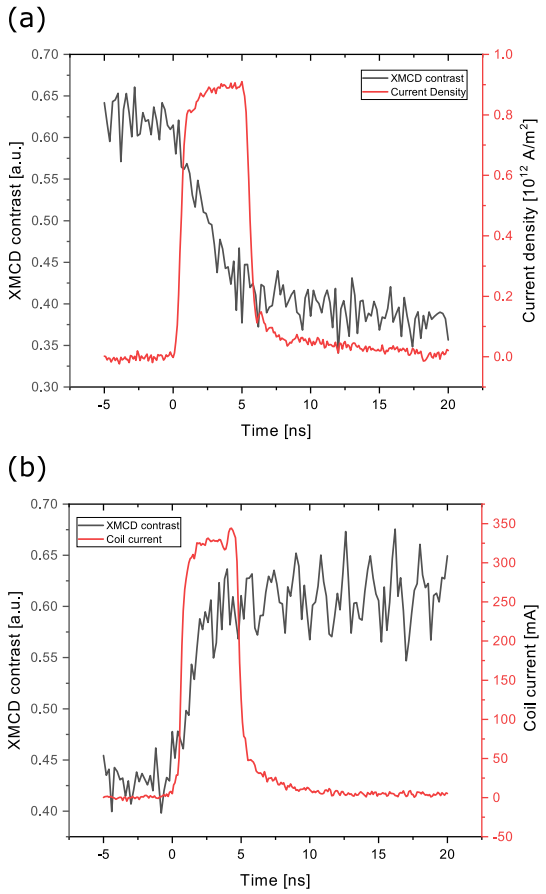

Figure 4: Time resolved XMCD contrast variation along the magnetic domain wall upon (a) the injection of a current across the microwire, and (b) upon the injection of a current across the Ω-shaped coil. The XMCD contrast variation was determined by integrating the area where the domain wall displacement occurs in the time-resolved images (marked by the red dashed lines in Figure 3. A delay-free motion of the magnetic domain wall can be observed for both the CIDWM and the FIDWM processes. From the time traces, a domain wall velocity of 50 m s^{-1} and of 100 m s^{-1} can be observed for the CIDWM and FIDWM processes respectively.

the magnetic field pulse or by the electrical current, remaining therefore normal to the wire axis (the presence of a pinning site at the bottom edge of the microwire does not seem to affect the dynamical motion of the domain wall). This seems, at a first glance, in contrast with the models proposed in Refs.[10,11], and with quasi-static experimental observations[21]. However, in agreement with the predictions reported in Ref.[12], microwires with a large width (such as the 2 μm wires reported here) exhibit a long transient before reaching a steady-state motion with a defined domain wall tilt. At the start of such transient, fitting our experimental observations, the motion of the domain wall can be approximated as tilt-free. Therefore, a possible approach to reduce the effect of domain wall tilting, even in the presence of a pinning site at the edge of the microwire, while still keeping a reliable domain wall motion could be to employ a train of short current/field pulses as opposed to a long current/field pulse. The absence of an incubation time and the negligible inertia of these domain walls will guarantee that the short current/field pulses will displace the domain wall, whilst however being too fast to cause a sizable tilting of the domain wall. The application of a train of short current/field pulses could then be employed for long-distance displacement of the magnetic domain walls. This motion protocol is similar to the one reported in Ref.[21], where it was observed that short current pulses lead to a different behavior of the domain wall motion if compared to longer current pulses.

In conclusion, we have reported on the time-resolved imaging of the current- and field-induced domain wall dynamics in microwires fabricated out of Pt/$Co_{68}B_{32}$/Ir multilayered superlattice stacks exhibiting interfacial DM interaction at high spatial (25 nm) and temporal (50-70 ps) resolution using time-resolved STXM with a time step of 200 ps for the time-resolved images. In particular, the domain wall motion under the application of short (5 ns) current and (4 ns) magnetic field pulses was investigated. For both the current- and field-induced motion, the absence of an incubation time (within the available time step of 200 ps) was observed, suggesting a low inertial mass for the Néel domain walls stabilized in the Pt/$Co_{68}B_{32}$/Ir films. Furthermore, the absence of a tilting of the Néel domain walls when displaced by the short current/field pulses was observed, providing a possible motion protocol enabling a long-range tilt-free motion of the domain walls.

The substantial improvement in the time-resolved imaging that we report here combined with the insensitivity of STXM imaging to the surface potential of the sample will allow for the investigation of a wide range of current densities and pulse durations. Future measurements with longer pulse durations can e.g. be aimed at the investigation of the domain wall tilting process as a function of the pulse duration, or of the acceleration and deceleration processes of the magnetic domain walls in larger wires[10].

Acknowledgement

SF conceived the experiment, with input from JR, SW, KZ, and CHM. SF and KZ designed the sample. KZ grew the Pt/$Co_{68}B_{32}$/Ir multilayer superlattice stacks. KZ, AVS, and SAN characterized the magnetic properties of the Pt/$Co_{68}B_{32}$/Ir multilayer superlattice stacks. SF lithographically patterned the samples. SF, SW, SM, and JR performed the time-resolved STXM experiments. SF, with SW and JR, analyzed the time-resolved data. SF wrote the manuscript, which was then discussed with all authors.

This work was performed at the PolLux (X07DA) endstation of the Swiss Light Source, Paul Scherrer Institut, Villigen, Switzerland. The research leading to these results has received funding from the European Community's Seventh Framework Programme (FP7/2007-2013) under grant agreement No. 290605 (PSI-FELLOW/COFUND), and the European Union's Horizon 2020 Project MAGicSky (Grant No. 665095). The authors thank P. Gambardella for helpful discussions.

References

(1) Ralph, D.; Stiles, M. *Journal of Magnetism and Magnetic Materials* **2008**, *320*, 1190.

(2) Hayashi, M.; Thomas, L.; Moriya, R.; Rettner, C.; Parkin, S. *Science* **2008**, *320*, 209.

(3) Gambardella, P.; Miron, I. *Philosophical Transactions of the Royal Society A* **2011**, *369*, 3175.

(4) Miron, I.; Moore, T.; Szambolics, H.; Buda-Prejbeanu, L.; Auffret, S.; Rodmacq, B.; Pizzini, S.; Vogel, J.; Bonfim, M.; Schuhl, A.; Gaudin, G. *Nature Materials* **2011**, *10*, 419.

(5) Ryu, K.-S.; Thomas, L.; Yang, S.-H.; Parkin, S. *Nature Nanotechnology* **2013**, *8*, 527.

(6) Parkin, S.; Yang, S.-H. *Nature Nanotechnology* **2015**, *10*, 195.

(7) Lo Conte, R.; Martinez, E.; Hrabec, A.; Lamperti, A.; Schulz, T.; Nasi, L.; Lazzarini, L.; Mantovan, R.; Maccherozzi, F.; Dhesi, S. S.; Ocker, B.; Marrows, C. H.; Moore, T. A.; Kläui, M. *Physical Review B* **2015**, *91*, 014433.

(8) Vogel, J.; Bonfim, M.; Rougemaille, N.; Boulle, O.; Miron, I. M.; Auffret, S.; Rodmacq, B.; Gaudin, G.; Cezar, J. C.; Sirotti, F.; Pizzini, S. *Physical Review Letters* **2012**, *108*, 247202.

(9) Taniguchi, T.; Kim, K.-J.; Tono, T.; Moriyama, T.; Nakatani, Y.; Ono, T. *Applied Physics Express* **2015**, *8*, 073008.

(10) Torrejon, J.; Martinez, E.; Hayashi, M. *Nature Communications* **2016**, *7*, 13533.

(11) Boulle, O.; Rohart, S.; Buda-Prejbeanu, L.; Jue, E.; Miron, I.; Pizzini, S.; Vogel, J.; Gaudin, G.; Thiaville, A. *Physical Review Letters* **2013**, *111*, 217203.

(12) Jue, E.; Thiaville, A.; Pizzini, S.; Miltat, J.; Sampaio, J.; Buda-Prejebeanu, L.; Rohart, S.; Vogel, J.; Bonfim, M.; Boulle, O.; Auffret, S.; Miron, I.; Gaudin, G. *Physical Review B* **2016**, *93*, 014403.

(13) Schönhense, G. *Journal of Physics: Condensed Matter* **1999**, *11*, 9517.

(14) Zeissler, K.; Mruczkiewicz, M.; Finizio, S.; Raabe, J.; Shepley, P. M.; Sadovnikov, A. V.; Nikitov, S. A.; Fallon, K.; McFadzean, S.; McVitie, S.; Moore, T. A.; Burnell, G.; Marrows, C. H. *Scientific Reports* **2017**, *7*, 15125.

(15) Legrand, W.; Chauelau, J.-Y.; Maccariello, D.; Reyren, N.; Colling, S.; Bouzehouane, K.; Jaouen, N.; Cros, V.; Fert, A. *arXiv:1712.05978v2* **2018**,

(16) Vansteenkiste, A.; Leliaert, J.; Dvornik, M.; Helsen, M.; Garcia-Sanchez, F.; Van Waeyenberge, B. *AIP Advances* **2014**, *4*, 107133.

(17) Raabe, J.; Tzvetkov, G.; Flechsig, U.; Böge, M.; Jaggi, A.; Sarafimov, B.; Vernooij, M. G. C.; Huthwelker, T.; Ade, H.; Kilcoyne, D.; Tyliszczak, T.; Fink, R. H.; Quitmann, C. *Review of Scientific Instruments* **2008**, *79*, 113704.

(18) Schütz, G.; Wagner, W.; Wilhelm, W.; Kienle, P.; Zeller, R.; Frahm, R.; Materlik, G. *Physical Review Letters* **1987**, *58*, 737.

(19) Finizio, S.; Wintz, S.; Watts, B.; Raabe, J. *Microscopy and Microanalysis* **2018**, *24*, 452.

(20) Puzic, A.; Korhonen, T.; Kalantari, B.; Raabe, J.; Quitmann, C.; Jüllig, P.; Bommer, L.; Goll, D.; Schütz, G.; Wintz, S.; Strache, T.; Körner, M.; Marko, D.; Bunce, C.; Fassbender, J. *Synchrotron Radiation News* **2010**, *23*, 26.

(21) Garg, C.; Pushp, A.; Yang, S.-H.; Phung, T.; Hughes, B.; Rettner, C.; Parkin, S. *Nano Letters* **2018**, *18*, 1826.